Case Studies in Thermal Engineering 71 (2025) 106205

Contents lists available at ScienceDirect

Case Studies in Thermal Engineering

journal homepage: www.elsevier.com/locate/csite

3E analysis and multi-objective optimization of a novel isobaric compressed air energy storage system with a gravity-enhanced air storage reservoir

Ruifeng Cao *, Zhe Wang, Hongliang Fan, Ziqi Chen

School of Energy and Power Engineering, Northeast Electric Power University, Jilin, 132012, China

ARTICLE INFO

Keywords:
Isobaric adiabatic compressed air energy storage
Gravity energy storage
Thermodynamic analysis
Economic analysis
Airbag

ABSTRACT

The advanced adiabatic compressed air energy storage (AA-CAES) system is a viable alternative for long term energy storage. The exergy loss during throttling is a major obstacle to performance improvement in AA-CAES system. This paper introduces a new gravity-assisted isobaric AA-CAES system. The air storage reservoir in proposed system consists of three parts: an abandoned vertical mineshaft, a heavy load, and an elastic airbag. By balancing the supporting force generated by the high-pressure air with the gravity of the heavy load, isobaric air charging and discharging process is achieved. Thermodynamic and economic models are developed. The results show that under the optimized design condition, the air and occupied space energy storage density are 2.68 kWh/m^3 and 2.29 kWh/m^3, respectively. The energy efficiency and exergy efficiency are 87.10 % and 70.07 %, respectively. The exergy destruction is mainly due to irreversible exergy losses in the heat exchangers. The dynamic payback period and levelized cost of energy are 8.36 years and 0.0804 $/kWh, respectively.

Nomenclature

A	Area, m^2	*Abbreviations*	
ATC	Annual total cost, M$	AA-CAES	Advanced adiabatic compressed air energy storage
ATP	Annual total profit, M$	ASR	Air storage reservoir
ATR	Annual total revenue, M$	C	Compressor
AR	Annual revenue, M$	CAES	Compressed air energy storage
c	Cost, $	CCES	Compressed CO2 energy storage
CELF	Constant escalation levelization factor, %	CV	Cold vessel
DPP	Dynamic payback period, years	D	Destruction
ENE	Energy efficiency, %	EES	Electrochemical energy storage
ESD	Energy storage density, kWh/m^3	GES	Gravity energy storage
Ėx	Exergy, kW	HV	Hot vessel
EXE	Exergy efficiency, %	HX	Heat exchanger
g	Gravitational acceleration	I-CAES	Isobaric compressed air energy storage
h	Specific enthalpy, kJ/kg	IA-CAES	Isobaric adiabatic compressed Air energy storage
H	Height, m	IC	Intercooler

(*continued on next page*)

* Corresponding author.
E-mail address: ruifengcao@neepu.edu.cn (R. Cao).

https://doi.org/10.1016/j.csite.2025.106205
Received 22 September 2024; Received in revised form 7 April 2025; Accepted 26 April 2025
Available online 28 April 2025

(*continued*)

Nomenclature			
i_r	Discount rate, %	IH	Interheater
IRR	Internal rate of return, %	PHS	Pumped hydro storage
LCOE	Levelized cost of energy, $/kWh	T	Turbine
m	Mass flow rate, kg/s	V	Valve
M	Mass, kg	***Subscripts***	
N_C	Number of compressors	0	Reference state
N_d	Number of operating days per year, day	1	Ambient state
N_T	Number of air turbines	a	Air
N_y	Service life-years of the system, year	bl	Building and land
NPV	Net present value, M$	char	Charging process
p	Pressure, MPa	di	Direct
P	Power, kW	dischar	Discharging process
Q	Heat, kW	e	Electricity
r	Nominal escalation ratio, %	ele	Electrical equipment
R	Radius, m	hw	Hot water
s	Specific entropy, kJ/(kg·K)	HL	Heavy load
t	Time, hour	HU	Hot user
T	Temperature, °C or K	HV	Hot vessel
V	Volume, m^3	indi	Indirect
Greek symbols		inst	Installation
β	Pressure ratio	inv	Investment
δ	Pressure loss coefficient	moc	Monitoring and control
ε	Heat exchanger efficiency	opm	Operation and maintenance
η	Isentropic efficiency	os	Occupied space
ξ	Heat loss coefficient	pip	Piping
ρ	Density, kg/m^3	te	Total equipment
φ	Operation and maintenance factor	w	Water

1. Introduction

Globally, the incidence of extreme weather phenomena has escalated in recent years. The World Weather Attribution Organization said this is a visual reflection of global warming. Emissions of greenhouse gases from human activities are primarily responsible for the escalation in severity and occurrence rate of extreme weather events. Reducing carbon emissions has become a primary prerequisite for the development of all countries and decarbonization of the electricity sector system is essential for sustainable social and economic development [1]. Expanding the contribution of renewables in the energy mix effectively diminishes fossil fuel consumption and lowers emissions, but the problem of their high intermittency remains a great challenge [2]. Therefore, to utilize renewable energy sources more widely and efficiently, there is an urgent need for an energy storage technology that is capable of flexible scheduling and long-term energy storage [3].

Long-term energy storage approaches are commonly bifurcated into physical and chemical energy storage methods. Physical energy storage is mainly pumped hydro storage (PHS) [4,5], compressed air energy storage (CAES) [6,7]and gravity energy storage (GES) [8]. Chemical energy storage is mainly electrochemical energy storage (EES) [9–11]. In recent years, CAES technology stands out as a viable and promising contender in the energy storage sector due to its less restriction by geographical location, fast response time and low investment cost. From the perspectives of both volume and pressure of the air storage reservoir (ASR) of CAES system, CAES can be further categorized into two types: isovolumetric CAES and isobaric CAES. In an isovolumetric configuration of CAES, the ASR's dimensions stay unaltered, but the operational pressure shifts through charging or discharging cycles. On the contrary, in an isobaric configuration of CAES, the compressed air has a constant pressure during the charging or discharging processes and the air storage reservoir has a variable volume.

When a CAES system is operated in the isobaric mode, the compressor and turbine can operate efficiently and stably at their rated operating conditions. The high-pressure air stored in the ASR can be almost completely utilized during the discharging process, which improves the system efficiency. Nowadays, isobaric adiabatic compressed air energy storage (IA-CAES) system has been emphasized by some scholars. Chen et al. [12] introduced an innovative IA-CAES system utilizing a volatile fluid. In the system's arrangement, the storage container is partitioned by a movable piston into two distinct sections: one designated for air retention and the other for the infusion of a suitable volatile substance. While charging, the volatile fluid is kept at the desired pressure by waste heat thus keeping the system pressure constant. Odukomaiya et al. [13] designed and built a small experimental setup to verify the effectiveness of the liquid piston to compress or expand the gas for energy storage. It was discovered that enhancing the rate of thermal energy transfer from the stored fluid can improve system efficiency. In light of this, a method for improving heat transfer was suggested to achieve nearly isothermal and isobaric operations during compression and expansion. Zhang et al. [14] introduced a system that combines CAES and compressed CO2 energy storage (CCES). Constant-pressure operation of the system was ensured by placing a CCES flexible airbag into the CAES storage chamber. The technical and economic analysis confirmed that the storage cost and system efficiency were 0.1491 $/kWh and 67.47 %, respectively. Zhang et al. [15] proposed a pressure stabilization unit that utilizes the carbon dioxide phase change process to maintain a constant system pressure. Computational simulations of this system's thermodynamic and economic profiles reveal that its efficiency rates at 69.92 % and its storage costs average at $0.1332/kWh. Compared to an isovolumetric system with the

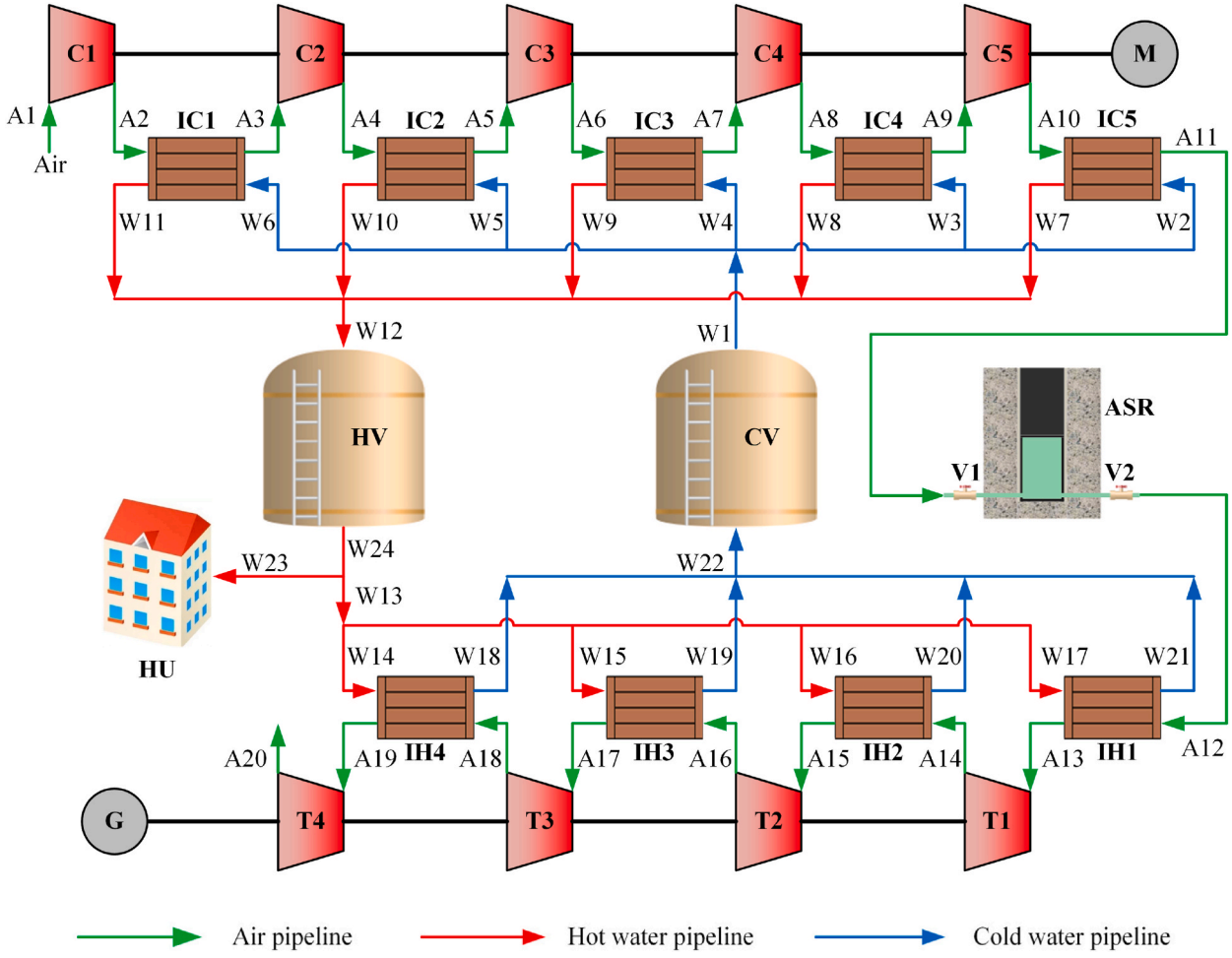

Fig. 1. Diagram of the proposed IA-CAES system.

same efficiency, the average storage cost decreased by 0.0138$/kWh and the volume of the air storage room was reduced by 31.86 %. To tackle the freshwater needs in coastal regions, Zhao et al. [16] introduced a hybrid system for small-scale electricity and freshwater supply based on the principle of energy cascade utilization. Utilizing low-grade heat from the charging and discharging of the IA-CAES system to generate freshwater. Simulation data suggests that within the specified design parameters, the total produced freshwater mass and the average cost of water are 851.77 kg and 0.57$/ton, respectively. Nabat et al. [17] conducted an extensive study of IA-CAES in terms of energy, exergy, and economy. In addition, thermodynamic and economic performances were analyzed by artificial neural networks and genetic algorithms. The proposed reference system recorded electrical, round-trip, and exergy efficiencies of 65.63 %, 68.28 %, and 66.01 %, respectively, based on the calculations. The total system cost is 21.15 $/GJ, while its average power cost value is 190.4 $/MWh. The system has a payback period of about 5.11 years and an eventual profit of about $40 million. Bartela et al. [18] introduced the concept of two systems, non-isobaric low-pressure reservoirs and isobaric high-pressure storage tanks, in the shafts of abandoned mines. Evaluated the pros and cons of the system, evaluated the required tank volume and the storage capacity, and analyzed the geometry of the mine. The results demonstrate the potential and effectiveness of the system. Zhang et al. [19] introduced an energy storage technique for gravity-enhanced CAES systems. System performance simulations executed in Thermoflex V29 suggested that theoretical energy storage efficiency was anticipated to be between 63.58 % and 65.50 %, and that the pressure for energy storage ought to be situated between 4 and 10 MPa. Stanek et al. [20] suggested a groundbreaking system for energy storage based on isobaric compressed carbon dioxide. In addition, the basic parameters of the installation are determined by thermodynamic analysis. Du et al. [21] devised an elastic isobaric strain energy compressed air storage device utilizing superelastic rubber. Explored and evaluated the impact of crucial factors on system efficacy during the processes of charging or discharging. In addition, the device's charging or discharging traits were evaluated. The findings indicate that the device has an average energy storage efficiency of 76.9 % and a volumetric energy density of 309.48 kJ/m^3, outperforming conventional rigid air storage reservoir by a factor of two. Rolland et al. [22] introduced a concept of IA-CAES system based on Pressure Equalization Module. The module is filled with a phase change material, and during charging and discharging, the phase change material is condensed and evaporated, respectively. Due to the change in volume air can achieve isobaric storage. Mazloum et al. [23] modeled the economics and thermodynamics of the IA-CAES

system using Dyloma. Findings demonstrate the system's energy density is 11.9 kWh/m^3 and the storage efficiency is 55.1 %. Wang et al. [24] presented a I-CAES system device by utilizing nonlinear cam transform mechanism and compressed gas energy storage. The outcomes suggest the new IA-CAES device has excellent constant voltage characteristics and energy-saving performance.

For such a system, multi-objective optimization is vital to find the best design performance. Alirahmi et al. [25] performed four multi-objective optimization programs based on MOPSO, NSGA-II, PESA-II, and SPEA2 algorithms for a hybrid system consisting of compressed air energy storage, a Brayton cycle, and a hydrogen production unit. It is concluded that the system has an exergy round trip efficiency of 60.4 % and a total cost rate of 117.5 $/GJ at the optimum solution. Özen et al. [26] conducted a multi-objective optimization for an AA-CAES system, the exergy efficiency and average unit product-exergy destruction cost are 94.58 % and 59.51$/GJ, respectively. Yao et al. [27] used multi-objective optimization to find the optimal parameter settings for a novel system that couples compressed air energy storage with chemical energy storage. 42.96 % of exergrtic round trip efficiency and 105.28 $/kWh of levelized cost of energy are obtained. Alirahmi et al. [28] conducted multi-objective optimization for a novel compressed air energy storage system hybridized with solar and desalination units, resulting in 48.7 % of round trip efficiency and a total cost of 3056 $/h.

Previous investigations indicate that the advancement of IA-CAES possesses significant potential. However, there is still a large gap in system design and analysis compared to advanced adiabatic compressed air energy storage (AA-CAES). For the AA-CAES system, the ASR is just a storage space with constant volume and it is relatively simple for operation. But the ASR operating at the constant pressure is the key component of the IA-CAES system. At present, most of the designs for constant-pressure ASR are underwater or piston structures. The operation of such an ASR is quite complex. Besides, the indicators for evaluating the system's technical and economic aspects are relatively few. Usually, additional auxiliary equipment is need to construct an IA-CAES system, which should be carefully considered during the economic analysis. In light of the issues mentioned earlier, this paper proposes a novel IA-CAES system that combines GES and AA-CAES. Energy, exergy and economic analysis are conducted to verify the feasibility of the system. The contributions and main innovations of this paper are summarized below.

- A novel IA-CAES system combining GES and AA-CAES is proposed. By designing a novel isobaric air storage reservoir, the system achieves isobaric operation. An abandoned vertical mine shaft is used as the air storage reservoir to maximize the land use. In addition, upon completion of the discharging phase, the air that has been stored can be entirely expelled, improving the energy storage density.
- A comprehensive description of thermodynamic and economic models of the proposed system is provided. By applying the NSGA-II multi-objective optimization algorithm, the optimal solution for the key parameters was obtained to be considered as the design condition of the system. The system performance indicators are calculated under the optimized design conditions to prove its feasibility.
- The study probes into how key variables affect system efficiency.

2. System description

Fig. 1 shows the diagram of the proposed IA-CAES system. During the charging phase, the excess power from wind and/or photovoltaic, or the valley power from the grid is stored through driving the compressors. The ambient atmosphere is transformed into high-pressure air (state point A11) and stored in the air storage reservoir (ASR). The process of five-stage sequential compression (C1-C5) is used to reduce energy consumption, and five intercoolers (IC1-IC5) is employed to capture the compression heat. The cool water, origination from the cold vessel (CV), is first warmed in the intercooler, resulting in the production of hot water that is subsequently collected in the hot vessel (HV). During the discharge phase, the stored high-pressure air (state point A12) is released from the air storage reservoir. Four-stage reheating is employed to enhance the power generation. Before entering the turbines (T1-T4), the hot water from the hot vessel (HV) heats the air in the interheater (IH1-IH4). In addition, the remainder of the hot water (state point W23) is supplied to the other heat users.

The isobaric air storage reservoir is the most critical component in the system. The main body of the air storage reservoir consists of three parts: an abandoned vertical mineshaft, a heavy load, and an elastic airbag. The elastic airbag is located at the bottom of the mineshaft and the heavy load is installed above the airbag. During the charging phase, the valve V1 opens and the valve V2 closes. The high-pressure air enters the airbag. With the continuous filling of air, the volume of the airbag increases continuously, leading to the increase in the height of the airbag. However, due to the constant weight of the heavy load and the constant contact area between the heavy load and airbag, the airbag's pressure level is unaltered during the charging operation, achieving an isobaric air charging process. Upon completion of the charging procedure and reaching the intended peak volume, the airbag is fully charged, symbolizing the fulfillment of its designed maximum capacity. During the discharging phase, the valve V2 opens and the valve V1 closes. With the action of gravitational potential energy of the heavy load, the air is squeezed out from the airbag. By the same principle mentioned above, an isobaric air discharging process can be achieved. The airbag is fully discharged when its volume reaches the designed minimum value and the discharging process is over.

3. Methodology

In this section, the energy and exergy analysis models for the system based on the first and second laws of thermodynamics are established and the thermodynamic performance indices are introduced. Furthermore, the economic model and economic evaluation indices for the system are presented.

Table 1
Energy balance equation of each component of proposed system.

Component	Energy equation	Ref.
Compressor	$P_C = \sum_{i=1}^{5} P_{C,i} = \sum_{i=1}^{5} m_{a,char}(h_{a,out,i} - h_{a,in,i}) = \frac{1}{\eta_C}\sum_{i=1}^{5} m_{a,char}(h_{a,out,s,i} - h_{a,in,i})$ $\beta_{C,i} = \frac{1}{(1-\delta)}\sqrt[5]{\frac{p_{ASR}}{p_1}}$	[30]
Turbine	$P_T = \sum_{i=1}^{4} P_{T,i} = \sum_{i=1}^{4} m_{a,dischar}(h_{a,in,i} - h_{a,out,i}) = \eta_T \sum_{i=1}^{4} m_{a,dischar}(h_{a,in,s,i} - h_{a,out,i})$ $\beta_{T,i} = (1-\delta)\sqrt[4]{\frac{p_{ASR}}{p_1}}$	[30]
Intercooler	$Q_{IC,i} = m_{a,char,i}(h_{a,in,i} - h_{a,out,i}) = m_{w,char,i}(h_{w,in,i} - h_{w,out,i})$ $T_{a,out,i} = T_{a,in,i} - \varepsilon(T_{a,in,i} - T_{w,in,i})$ $T_{w,out,i} = T_{w,in,i} + \varepsilon(T_{a,in,i} - T_{w,in,i})$	[31,32]
Interheater	$Q_{IH,i} = m_{a,dischar,i}(h_{a,in,i} - h_{a,out,i}) = m_{w,dischar,i}(h_{w,in,i} - h_{w,out,i})$ $T_{a,out,i} = T_{a,in,i} + \varepsilon(T_{w,in,i} - T_{a,in,i})$ $T_{w,out,i} = T_{w,in,i} - \varepsilon(T_{w,in,i} - T_{a,in,i})$	[31,32]
Air storage reservoir	$h_{a,out} = h_{a,in}$	
Hot vessel	$h_{w,out} = h_{w,in}(1-\xi)$	

3.1. Assumptions

To analyze the system more efficiently and simply, the following assumptions are utilized.

(1) The power dissipation of all pumps is neglected [14].
(2) The effects of kinetic and potential energy are ignored [17].
(3) Pressure and heat loss from all pipes in the system are neglected [12].
(4) The air used in the study is considered the ideal gas [29].
(5) The compressor and air turbine operate with a constant isentropic efficiency [17].

3.2. Energy analysis

Based on the assumptions, the energy balance model of each components of the proposed system are listed in Table 1. During the compression phase, it is assumed that each compressor operates with an identical compression ratio. A pressure loss coefficient δ is adopted to model the air pressure loss in the intercooler. Similarly, for the expansion process, it is considered that each turbine has the same expansion ratio. A pressure loss coefficient (δ) is also adopted to model the air pressure loss in the interheater. For the intercooler and interheater, the heat exchanger efficiency (ε) is considered. For the hot vessel, a heat loss coefficient (ξ) is considered.

For the air storage reservoir, it is considered that there is an absence of thermal interaction between the air and the surroundings and thus, the air temperature within the air storage reservoir aligns with the air temperature at the intake. In addition, it is assumed that the radius of the airbag and heavy load are same and equal to the radius of the shaft. Therefore, the required maximum volume and height of the airbag can be calculated from

$$V_{airbag} = \frac{3600}{\rho_{ASR}} \int_0^{t_{char}} m_{a,char} dt = \frac{3600}{\rho_{ASR}} \int_0^{t_{dischar}} m_{a,dischar} dt \tag{1}$$

$$H_{airbag} = \frac{V_{airbag}}{\pi R_{shaft}^2} \tag{2}$$

The required volume and height of the heavy load can be obtained by balancing the supporting force generated by the high-pressure air within the airbag with the gravity of the heavy load:

$$V_{HL} = \frac{p_{ASR}}{\rho_{HL} g} \pi R_{shaft}^2 \tag{3}$$

$$H_{HL} = \frac{p_{ASR}}{\rho_{HL} g} \tag{4}$$

The height of the shaft can be obtained as

$$H_{shaft} = H_{airbag} + H_{HL} \tag{5}$$

The energy storage density (*ESD*) offers valuable insights into a system's capacity for efficient energy storage and utilization. In this study, two energy storage density are defined, namely air energy storage density (ESD_a) and occupied space energy storage density (ESD_{os}), determinable through the application of these equations [33]:

Table 2
Exergy destruction and efficiency of each component of the system.

Component	Exergy destruction	Exergy efficiency
Compressor	$\dot{E}x^{D}_{C,i} = P_{C,i} - \left(\dot{E}x_{C,out,i} - \dot{E}x_{C,in,i}\right)$	$EXE_{C,i} = \left(\dot{E}x_{C,out,i} - \dot{E}x_{C,in,i}\right)/P_{C,i}$
Turbine	$\dot{E}x^{D}_{T,i} = \dot{E}x_{T,in,i} - \dot{E}x_{T,out,i} - P_{T,i}$	$EXE_{T,i} = P_{T,i}/\left(\dot{E}x_{T,in,i} - \dot{E}x_{T,out,i}\right)$
Intercooler	$\dot{E}x^{D}_{IC,i} = \sum \dot{E}x_{IC,in,i} - \sum \dot{E}x_{IC,out,i}$	$EXE_{IC,i} = \left(\dot{E}x_{w,out,i} - \dot{E}x_{w,in,i}\right)/\left(\dot{E}x_{a,in,i} - \dot{E}x_{a,out,i}\right)$
Interheater	$\dot{E}x^{D}_{IH,i} = \sum \dot{E}x_{IH,in,i} - \sum \dot{E}x_{IH,out,i}$	$EXE_{IH,i} = \left(\dot{E}x_{a,out,i} - \dot{E}x_{a,in,i}\right)/\left(\dot{E}x_{w,in,i} - \dot{E}x_{w,out,i}\right)$
Air storage reservoir	$\dot{E}x^{D}_{ASR} = \dot{E}x_{ASR,in} - \dot{E}x_{ASR,out} = 0$	$EXE_{ASR} = \dot{E}x_{ASR,out}/\dot{E}x_{ASR,in} = 100\%$
Hot vessel	$\dot{E}x^{D}_{HV} = \dot{E}x_{HV,in} - \dot{E}x_{HV,out}$	$EXE_{HV} = \dot{E}x_{HV,out}/\dot{E}x_{HV,in}$

Table 3
Cost equations for the main components of the system.

Component	Cost equation	Ref.
Compressor	$C_{C,i} = \frac{71.1 m_{C,i}}{0.92 - \eta_{C,i}} \beta_{C,i} \ln\left(\beta_{C,i}\right)$	[39]
Turbine	$C_{T,i} = \frac{479.34 m_{T,i}}{0.92 - \eta_{T,i}} \ln\left(\beta_{T,i}\right)\left[1 + \exp\left(0.036 T_{T,in,i} - 54.4\right)\right]$	[40]
Intercooler	$C_{IC,i} = 12000\left(\frac{A_{IC,i}}{100}\right)^{0.6}$ $A_{IC,i} = \frac{m_w \Delta h}{K \Delta t_m}$ $\Delta t_m = \left[\left(T_{h,in,i} - T_{c,out,i}\right) + \left(T_{h,out,i} - T_{c,in,i}\right)\right]/2$	[41,42]
Interheater	$C_{IH,i} = 12000\left(\frac{A_{IH,i}}{100}\right)^{0.6}$	[41,42]
Air storage reservoir	$C_{ASR} = C_{airbag} + C_{HL} + C_{shaft}$ $C_{airbag} = 0.75 \times 1.218 \exp\left[2.631 + 1.3676 \ln V_{airbag} - 0.06309\left(\ln V_{airbag}\right)^2\right]$ $C_{HL} = c_{HL} M_{HL} = c_{HL} \rho_{HL} V_{HL}$ $C_{shaft} = 2\pi R_{shaft}\left(H_{shaft} + R_{shaft}\right) c_{paint}$	[18]
Hot/cold vessel	$C_{HV/CV} = 5941.7\left(V_{HV/CV}\right)^{0.389}$	[43]

$$ESD_a = \frac{\int_0^{t_{dischar}} P_T dt}{V_{airbag}} \tag{6}$$

$$ESD_{os} = \frac{\int_0^{t_{dischar}} P_T dt}{V_{shaft}} \tag{7}$$

The energy efficiency (*ENE*) is specified by the quotient of the total energy discharged during the discharging phase and the total energy consumed throughout the charging phase [33]:

$$ENE = \frac{\int_0^{t_{dischar}} \left(P_T + P_{hw}\right) dt}{\int_0^{t_{char}} P_C dt} \tag{8}$$

3.3. Exergy analysis

The total exergy at any given state point can be expressed by multiplying the mass flow rate by the specific exergy [34]:

$$\dot{E}x = m[h - h_0 - T_0(s - s_0)] \tag{9}$$

The exergy analysis method is fundamentally predicated on the exergy balance equation. By applying an analogous approach as that used for the development of the energy equilibrium equation, the exergy equilibrium equation for individual components can be crafted. Given that exergy destruction is a concomitant of any irreversible process within a system, it is imperative to account for this phenomenon. Consequently, the exergy conservation equation for the *k*th component can be formulated as [35]:

$$\dot{E}x^{Q}_k + \sum \dot{E}x_{k,in} = \sum \dot{E}x_{k,out} + \dot{E}x^{W}_k + \dot{E}x^{D}_k \tag{10}$$

The exergy destruction and efficiency of each system component are delineated in Table 2 [36]. It is important to highlight that, in the scenario where the air storage reservoir is presumed to experience no heat transfer, the exergy destruction is null, consequently yielding an exergy efficiency of 100 %.

The exergy efficacy (*EXE*) is expressed as the comparison of the total exergy output from the discharge to the total exergy input from the charging stage [33]:

Table 4
Cost equations for the system construction.

Description	Cost function
Installation cost	$C_{inst} = 0.25C_{te}$
Monitoring and control cost	$C_{moc} = 0.08C_{te}$
Plumbing cost	$C_{pip} = 0.1C_{te}$
Electrical equipment cost	$C_{ele} = 0.1C_{te}$
Building and land cost	$C_{bl} = 0.14C_{te}$

$$EXE = \frac{\int_0^{t_{dischar}} (P_T + \dot{E}x_{hw})dt}{\int_0^{t_{char}} P_C dt} \tag{11}$$

3.4. Economic analysis

Economic analysis stands as a pivotal criterion for assessing the financial viability of an energy storage project and informing investment decisions. The model for calculating the costs and benefits of the system is presented to provide a basis for investment and operation decisions.

The total investment cost can be categorized into direct investment cost ($C_{inv,di}$) and indirect investment cost ($C_{inv,indi}$), which can be expressed as [30,37,38]:

$$C_{inv} = C_{inv,di} + C_{inv,indi} \tag{12}$$

$$C_{inv,di} = C_{te} + C_{inst} + C_{moc} + C_{pip} + C_{ele} + C_{bl} \tag{13}$$

$$C_{inv,indi} = 0.14C_{inv,di} \tag{14}$$

The comprehensive equipment acquisition cost (C_{te}) of the system, represents the aggregate expenditure on the procurement of its constituent principal components, which are listed in Table 3. During the analysis, the chemical engineering plant cost index (CEPCI) is utilized to adjust the procurement cost for every part of the system. The other system construction cost is given in Table 4.

The computation of the annual total cost (ATC) is delineated by Refs. [44,45]:

$$ATC = AC_{e,char} + AC_{opm} \tag{15}$$

$$AC_{e,char} = c_{e,char} \cdot P_C \cdot t_{char} \cdot N_d \cdot CELF \tag{16}$$

$$AC_{opm} = C_{inv} \cdot \varphi \cdot CRF \tag{17}$$

$$CELF = \frac{1+r}{i_r - r} \cdot \left[1 - \left(\frac{1+r}{1+i_r}\right)^{N_y}\right] \cdot CRF \tag{18}$$

$$CRF = \frac{i_r \cdot (1+i_r)^{Ny}}{(1+i_r)^{Ny} - 1} \tag{19}$$

The annual total revenue (*ATR*) can refer to the following calculations [44]:

$$ATR = AR_{e,dischar} + AR_{hw} \tag{20}$$

$$AR_{e,dischar} = c_{e,dischar} \cdot P_T \cdot t_{dischar} \cdot N_d \cdot CELF \tag{21}$$

$$AR_{hw} = c_{hw} \cdot P_{hw} \cdot t_{dischar} \cdot N_d \cdot CELF \tag{22}$$

The formula for gauging the system's annual total profit (*ATP*) is as follows [44]:

$$ATP = ATR - ATC \tag{23}$$

The total of the system's projected cash inflows and outflows over its lifetime when discounted to present value at the given discount rate is what is known as the net present value (*NPV*). When the *NPV* is greater than 0, it indicates that the system is earning more than the baseline return and the system is feasible. The *NPV* can be calculated by Ref. [46]:

$$NPV = \sum_{t=1}^{N_y} \left[\frac{ATP}{(1+i_r)^t}\right] - C_{inv} \tag{24}$$

To assess the economic viability of energy storage initiatives, the levelized cost of energy (*LCOE*) is derived by averaging the system's overall expenses across its total lifespan against its cumulative energy yield. Considering the discounting effect of time on

Table 5
Verification of system simulation results.

Items	Parameters	Present work	Reference	Error (%)
Input parameters	Ambient temperature (°C)	20	20	–
	Atmospheric pressure (kPa)	101.5	101.5	–
	Isentropic efficiency of compressors (%)	85	85	–
	Isentropic efficiency of turbines (%)	85	85	–
	Pressure loss coefficient in the IC/HT (%)	1	1	–
	Temperature in the ASR (°C)	20	20	–
	Pressure in the ASR (MPa)	4	4	–
Verification parameters	Energy efficiency (%)	65.88	63.58	3.62
	Exergy efficiency of first stage compressor (%)	88.08	89.91	−2.04
	Exergy efficiency of first stage turbine (%)	84.64	85.43	−0.92

Table 6
Basic energy parameters of the proposed system under design conditions.

Parameter	Unit	Value
Ambient temperature (T_0)	°C	25
Ambient pressure (p_0)	MPa	0.1
Pressure loss coefficient in ICs/IHs (δ)	%	3
Heat loss coefficient of hot vessel (ξ)	%	3
Charging time (t_{char})	hour	2
Discharging time ($t_{dischar}$)	hour	2
Radius of shaft (R_{shaft})	m	2
Density of heavy load (ρ_{HL})	kg/m^3	7870
Gravitational acceleration (g)	m/s^2	9.8
Total power generated by turbines (P_T)	kW	4000

money, the *LCOE* can be defined as [47]:

$$LCOE = \frac{\sum_{t=1}^{N_y} \frac{ATC}{(1+i_r)^t}}{N_d \sum_{t=1}^{N_y} \frac{\int_0^{t_{dischar}} (P_T + P_{hw}) dt}{(1+i_r)^t}} \tag{25}$$

The dynamic payback period (*DPP*) denotes the number of years needed to recoup the complete investment from annual net earnings, with the consideration of the monetary time value, through a calculated method, which is calculated by Ref. [33]:

$$NPV = \sum_{i=1}^{DPP} \left[\frac{ATP}{(1+i_r)^t} \right] - C_{inv} = 0 \tag{26}$$

Internal rate of return (*IRR*) is another very important economic evaluation index in addition to *NPV*, which can reflect the efficiency of the use of funds. The discount rate is the interest rate at which the *NPV* of the energy storage project's lifetime cash flows balances at zero and can be calculated by Ref. [46]:

$$NPV = \sum_{t=1}^{N_y} \left[\frac{ATP}{(1+IRR)^t} \right] - C_{inv} = 0 \tag{27}$$

4. Results and discussion

The energy, exergy, and economic models for the proposed system have been simulated using MATLAB software. The REFPROP 9.1 software is utilized to determine the thermal characteristics of both air and water.

4.1. Model validation

To affirm the trustworthiness of the system model, the calculated performance of some key components and the whole system are verified by juxtaposing these results against those reported in authoritative texts, under strictly controlled parameter conditions. Table 5 shows the comparison between the simulation results of this system and the results reported in Ref. [19]. The findings indicate that discrepancies between the two systems peak at below 4 %. Consequently, the model devised in this research is deemed highly accurate and trustworthy.

Table 7
Basic economic parameters of the proposed system under design conditions.

Parameters	Unit	Value	Ref.
Price of electricity for discharging period ($c_{e,dischar}$)	$/kWh	0.18	[17]
Price of paint (c_{paint})	$/m^2	11.1	[18]
Price of heavy load (c_{HL})	$/kg	0.1	[19]
Operating days per year (N_d)	day	350	[33]
Price of hot water (c_{hw})	$/kWh	0.018	[44]
Price of electricity for charging period ($c_{e,char}$)	$/kWh	0.04	[45]
Discount rate (i_r)	%	10	[50]
Nominal escalation ratio (r)	%	3	[51]
Operation and maintenance factor (φ)	%	6	[52]
Service life-years (N_y)	year	25	[53]

Table 8
Parameter settings and ranges for multi-objective optimization.

Parameter	Unit	Value
Air storage pressure (p_{ASR})	MPa	[3,5]
Heat exchanger efficiency (ε)	%	[80,90]
Compressor isentropic efficiency (η_C)	%	[82,89]
Turbine isentropic efficiency (η_T)	%	[82,89]

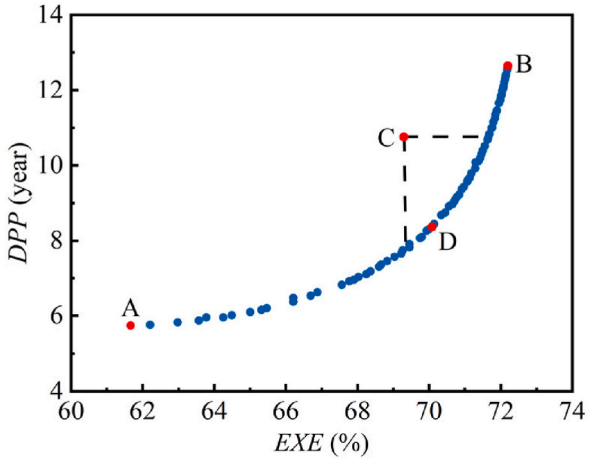

Fig. 2. Distribution of Pareto frontier solutions.

Table 9
Parameter setting after multi-objective optimization.

Parameter	Unit	Value
Air storage pressure	MPa	3.12
Heat exchanger efficiency	%	89.98
Compressor isentropic efficiency	%	88.29
Turbine isentropic efficiency	%	86.86

4.2. Design parameter determination through multi-objective optimization

In this study, a 4000kW/8000 kWh CAES system is considered. A detailed inventory of the system's design parameters is enumerated in Table 6 [3,16,19,48,49]. Table 7 enumerates the foundational economic parameters for the system evaluation. Table 8 shows the required parameter settings and their ranges for the multi-objective optimization process. The air storage pressure, compressor isentropic efficiency, heat exchanger efficiency and turbine isentropic efficiency are selected as decision variables.

In this paper, maximizing *EXE* and minimizing *DPP* are chosen as the objective function, which can be denoted as:

$$F = [\max(EXE), \min(DPP)]^{T} \tag{28}$$

Table 10
Simulated performance of proposed system under optimization conditions.

Parameter	Unit	Value
Total power consumption of compressors (P_c)	kW	5880.82
Total power generated by turbines (P_T)	kW	4000.00
Power of heating supply (P_{hw})	kW	1122.02
Air mass flow rate ($m_{a,char}$ and $m_{a,dischar}$)	kg/s	14.86
Maximum height of airbag (H_{airbag})	m	237.32
Maximum volume of airbag (V_{airbag})	m^3	2982.24
Height of heavy load (H_{HL})	m	40.44
Volume of heavy load (V_{HL})	m^3	508.21
Air energy storage density (ESD_a)	kWh/m^3	2.68
occupied space energy storage density (ESD_{os})	kWh/m^3	2.29
Energy efficiency (*ENE*)	%	87.10
Exergy efficiency (*EXE*)	%	70.07

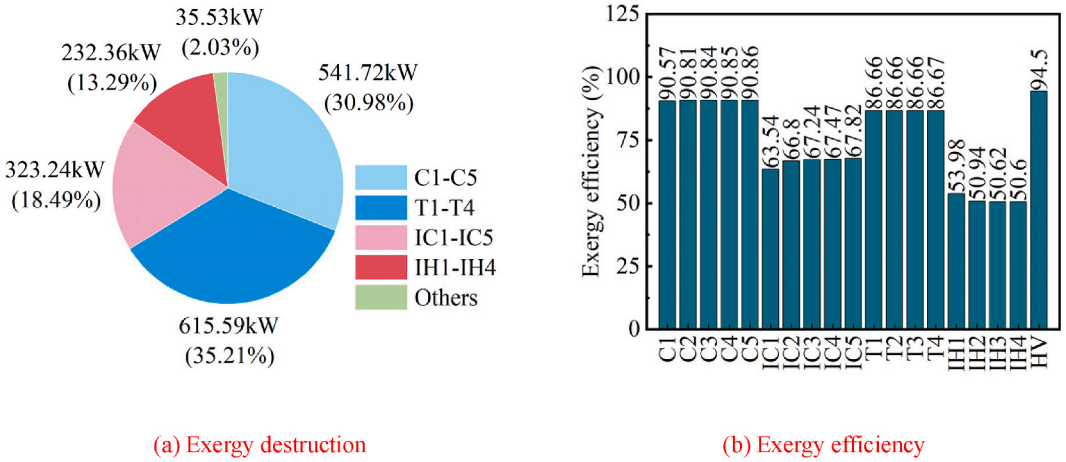

Fig. 3. Exergy destruction and Exergy efficiency of main components.

Table 11
Simulation results of the system economic analysis.

Parameters	Unit	Value
Total investment cost (C_{inv})	M$	2.45
Annual total cost (*ATC*)	M$	0.23
Annual total profit (*ATP*)	M$	0.45
Annual total revenue (*ATR*)	M$	0.68
Dynamic payback period (*DPP*)	year	8.36
Levelized cost of energy (*LCOE*)	$/kWh	0.0804
Net present value (*NPV*)	M$	1.60
Internal rate of return (*IRR*)	%	17.93

As a well-received technique, NSGA-II in the realm of multi-objective genetic algorithms is often deployed to seek out Pareto optimal solutions. By using the TOPSIS method to find the optimal solution within the solution set. Fig. 2 shows the Pareto optimal solution for *EXE* and *DPP* of the system. Point C shows the values of *EXE* and *DPP* under the specified design conditions given in Table 6. By the selection of the TOPSIS method, point D is the optimal solution. At point D of the system, the value of decision variables is delineated in Table 9.

4.3. Energy analysis

Based on the established models, Table A1 in the Appendix details the thermodynamic parameters for every state point within the proposed system and Table 10 gives the performance indicators of the proposed system under the condition of optimized parameters. During the charging process, the compressor incurs an energy usage of 5880.82 kW. The system's air flow rate is consistent at 14.86 kg/s during both the charging and discharging phases, thanks to equal timing for each. The power of heating is 1122.02 kW for 2 h. The ESD_a and ESD_{os} are 2.68 kWh/m^3 and 2.29 kWh/m^3, respectively. The *ENE* and *EXE* 87.10 % and 70.07 %, respectively. Additionally,

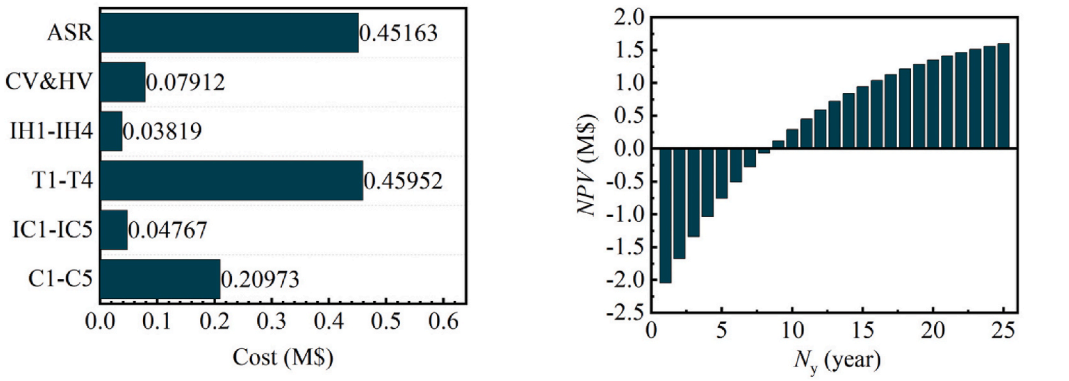

(a) Cost of system components (b) *NPV* profile per year for the system's lifecycle

Fig. 4. Results of economic analysis.

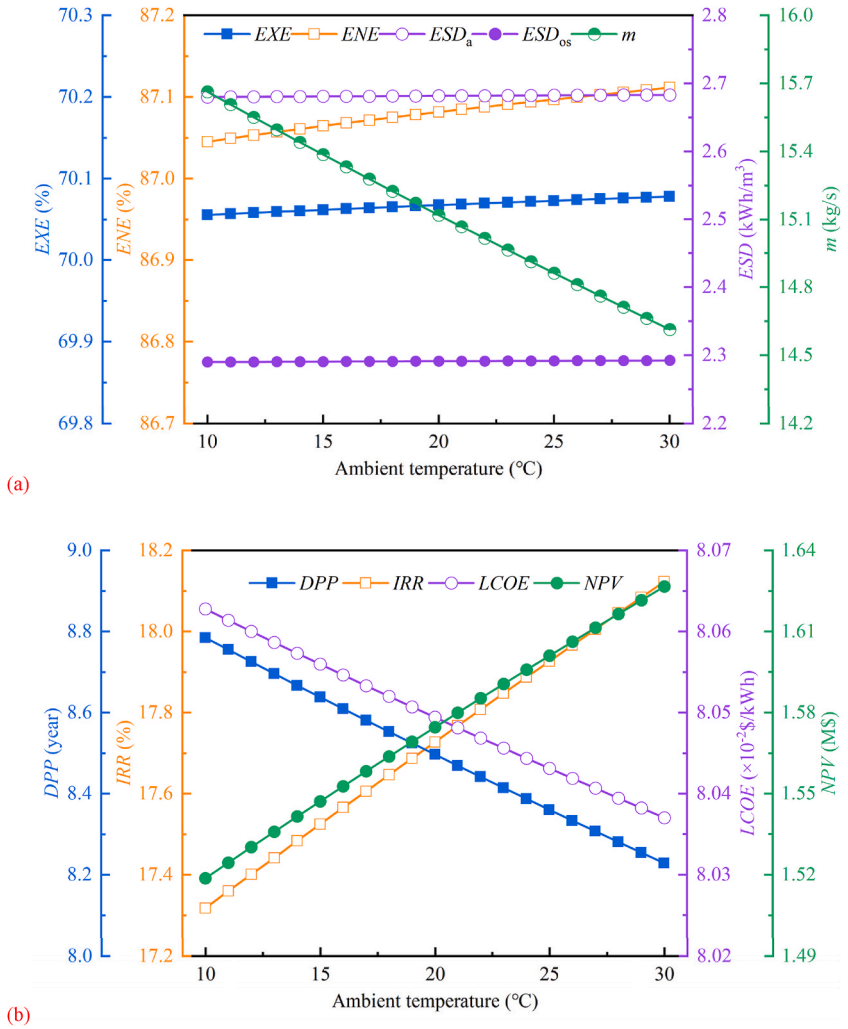

Fig. 5. Effect of ambient temperature on system performance: (a) *ENE*, *EXE*, *ESD*, and *m*; (b) *IRR*, *DPP*, *LCOE*, and *NPV*.

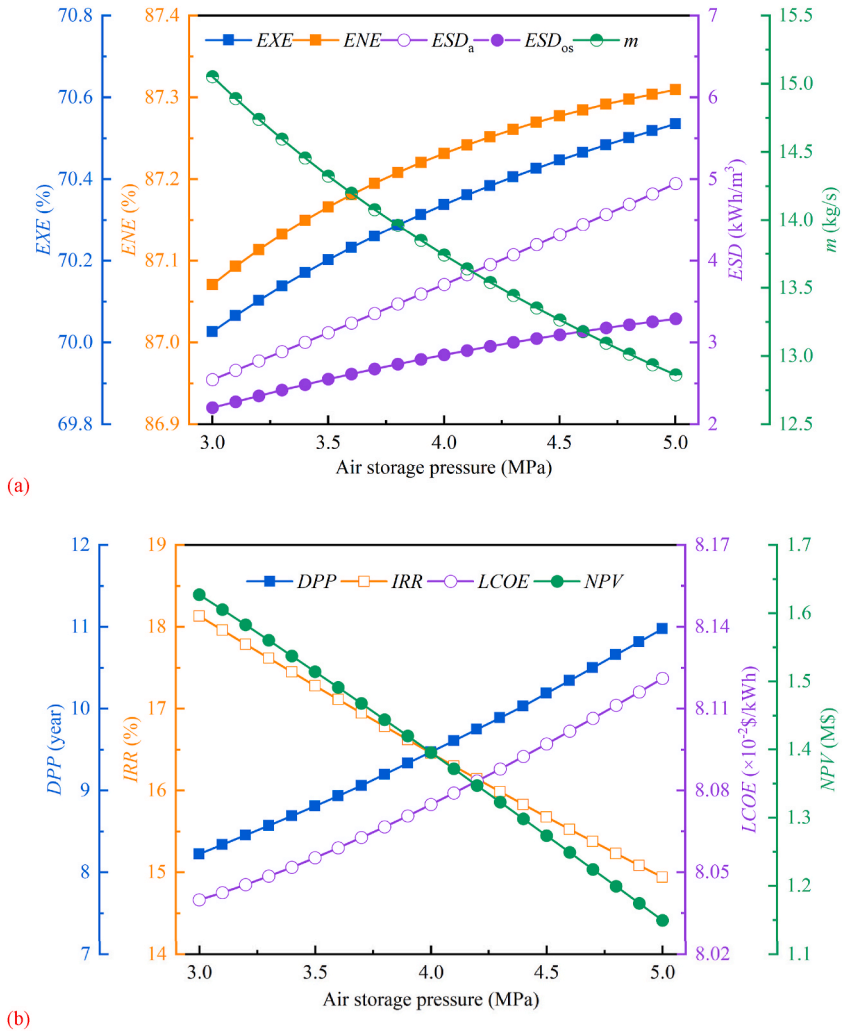

Fig. 6. Effect of air storage pressure on system performance: (a) *ENE*, *EXE*, *ESD*, and *m*; (b) *IRR*, *DPP*, *LCOE*, and *NPV*.

the required maximum volume and height of the airbag are 2982.24 m^3 and 237.32 m, respectively. The required volume and height of the heavy load are 508.21 m^3 and 40.44 m, respectively.

4.4. Exergy analysis

The exergy efficiency and exergy destruction rate of each component of the system is depicted in Fig. 3. The turbines and compressors are the two components with highest exergy destruction rates in the proposed system, accounting for 35.21 % (615.59 kW) and 30.98 % (541.72 kW) of the total, respectively. Next are the intercooler and interheater, which account for 18.49 % (323.24 kW) and 13.29 % (232.36 kW) of the total, respectively. The exergy destruction rate of other components is 35.53 kW, accounting for 2.03 % of total. Additionally, the exergy efficiency of the intercoolers and interheaters is significantly lower than other components, ranging between 50.60 % and 67.82 %. This phenomenon predominantly arises from the marked disparity in temperature between the heated and cooled fluids as they pass through the heat exchangers The *EXE* of compressors is generally above 90 % and that of turbines is generally above 86 %. The exergy efficiency of the HV is 94.50 %, which is caused by the heat loss.

The Sankey diagram of the system exergy flow process is given in Fig. A1 in the Section of Appendix. The complete exergy input for operation of the system is derived from the energy exhausted by the compressors, which is 100 %. The exergy output of the system including the power generated by the turbines, accounting for 68.02 % of exergy input and the exergy of hot water, accounting for 2.10 % of exergy input. The total exergy destruction of the system is the sum of components loss (29.72 %) and hot water loss (0.16 %) to the cold tank, which is 29.88 %.

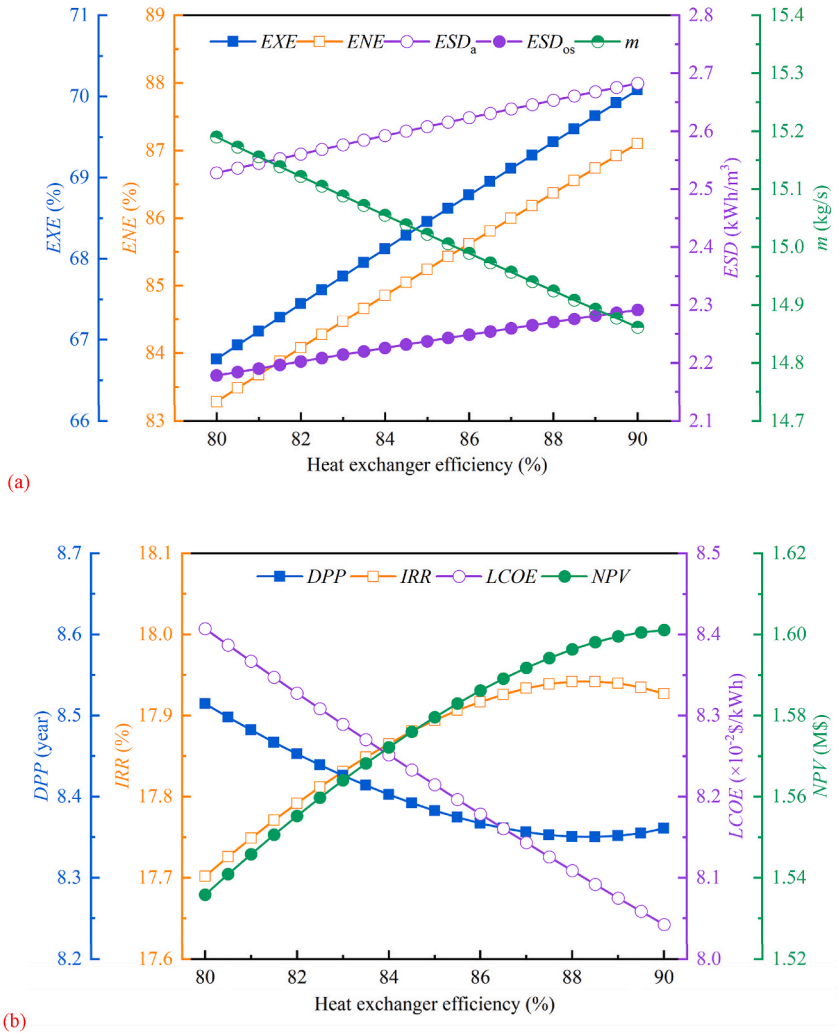

Fig. 7. Effect of heat exchanger efficiency on system performance: (a) *ENE*, *EXE*, *ESD*, and *m*; (b) *IRR*, *DPP*, *LCOE*, and *NPV*.

4.5. Economic analysis

Table 11 presents the economic analysis results of the proposed system under the condition of optimized parameters. The outcomes indicate that the overall investment cost of the system in the construction phase is 2.45 M$. The *ATR*, *ATC* and *ATP* of the system are 0.68 M$, 0.23 M$ and 0.45 M$, respectively. The *LCOE* is 0.0804 $/kWh, the *DPP* is 8.36 years, and the *IRR* is 17.93 %. The conclusions drawn from the study indicate that the proposed system displays remarkable economic performance and remarkable profitability.

Fig. 4 shows the results of economic analysis. Ascertained from Fig. 4a that the component with highest cost is the turbines, which amount to 0.45952 M$. The second one is the air storage reservoir, in which the heavy load accounts for most of the cost. Therefore, to reduce the total system cost, the priority is to find a material with high density and low price for the heavy load. Fig. 4b presents the *NPV* of the proposed system. It can be found that between eight and nine years, the *NPV* starts to be positive and the system starts to make a profit.

4.6. Parametric analysis

Parametric analysis, also known as sensitivity analysis, is a method of analyzing the effect of variation in the parameters of the system on the state or output of the system. It can also be used to understand which parameters have a greater effect on the system. In this subsection, parametric analyses are conducted.

4.6.1. Effect of ambient temperature

Fig. 5 presents the relationship between ambient temperature and system performance. As Fig. 5a illustrates, an elevation in

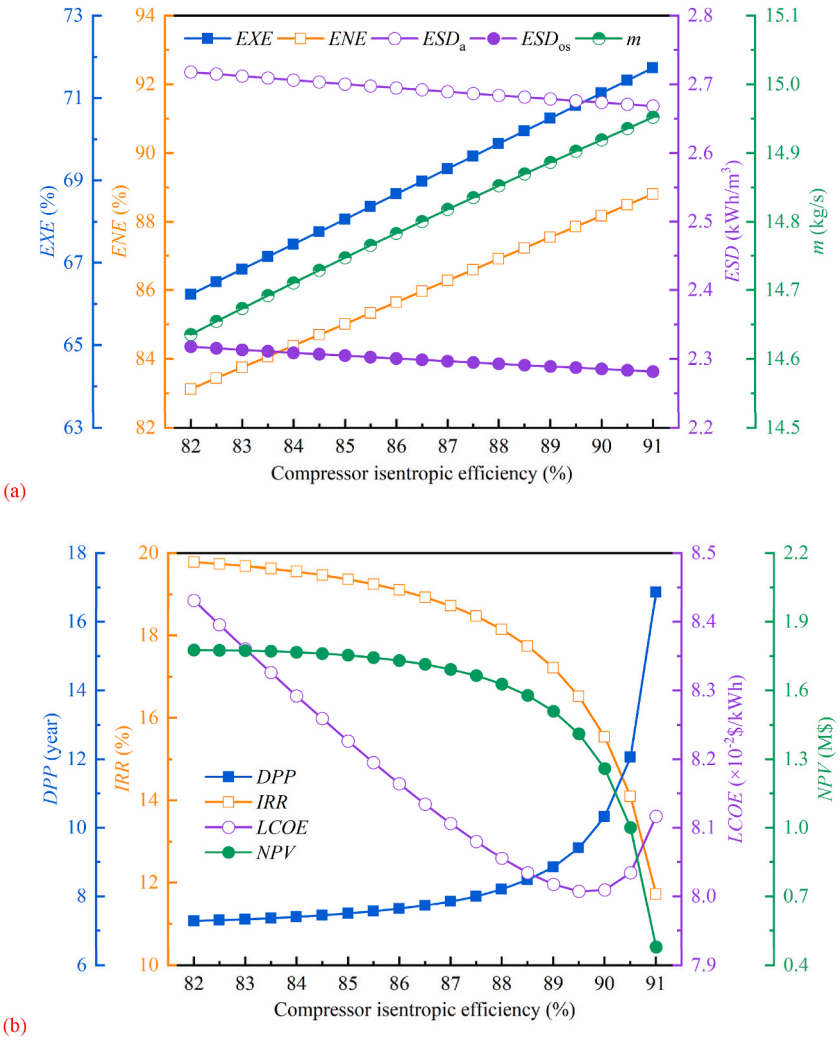

Fig. 8. Effect of compressor isentropic efficiency on system performance: (a) *ENE*, *EXE*, *ESD*, and *m*; (b) *IRR*, *DPP*, *LCOE*, and *NPV*.

ambient temperature results in an increase in compression heat temperature, further making the inlet air temperature of turbine higher. Thus, for the specified turbine power of 4 MW, as the ambient temperature rises from 10 °C to 30 °C, the required air mass flow decreases slightly from 15.66 kg/s to 14.61 kg/s. Meanwhile, though the total amount of stored air reduces, the volume reduction of airbag is very small and there is just a very small increase in *ESD*. Consequently, while the compressor's specific power draw escalates with a higher ambient temperature, the decline in air mass flow entails a minor dip in total consumption. Therefore, there is a slight increase in the *EXE* and *ENE*. As depicted in Fig. 5b, when the ambient temperature increases, *IRR* and *NPV* increase slightly while *DPP* and *LCOE* decrease slightly. This is because, according the cost equations given in Table 3, the decreased air mass flow results in the cost reduction of compressors, turbines, heat exchangers and air storage reservoir.

4.6.2. *Effect of air storage pressure*

Fig. 6 illustrates the impact of air storage pressure on system performance. Firstly, for the specified turbine power of 4 MW, elevated air storage pressure is bound to mean higher specific power generation of turbine and less air mass flow rate, which leads to the increases in *ESD*. A linear increase from 2.55 kWh/m^3 to 4.95 kWh/m^3 for ESD_a can be discovered when the pressure of air storage rises from 3 MPa to 5 MPa. Secondly, although higher air storage pressure means higher specific power consumption of compressor, the decreased air mass flow rate results in that the compressor power consumption is almost unchanged. Therefore, there is just a negligible change in the *ENE* and *EXE*. Regarding the state of the economy, according to the above analysis, higher air storage pressure means lower air mass flow rates, which results in a minor escalation in compressor expenses and a slight decrease in the cost of turbines and heat exchangers. However, higher air storage pressure causes a significant increase in the cost of heavy load. Therefore, as shown in Fig. 6b, *IRR* and *NPV* decrease while *LCOE* and *DPP* increase with the increase of the air storage pressure. The *LCOE* increases from 0.0804 $/kWh to 0.0812 $/kWh and the *DPP* increases from 8.04 years to 8.12 years as the air storage pressure increases from 3 MPa to

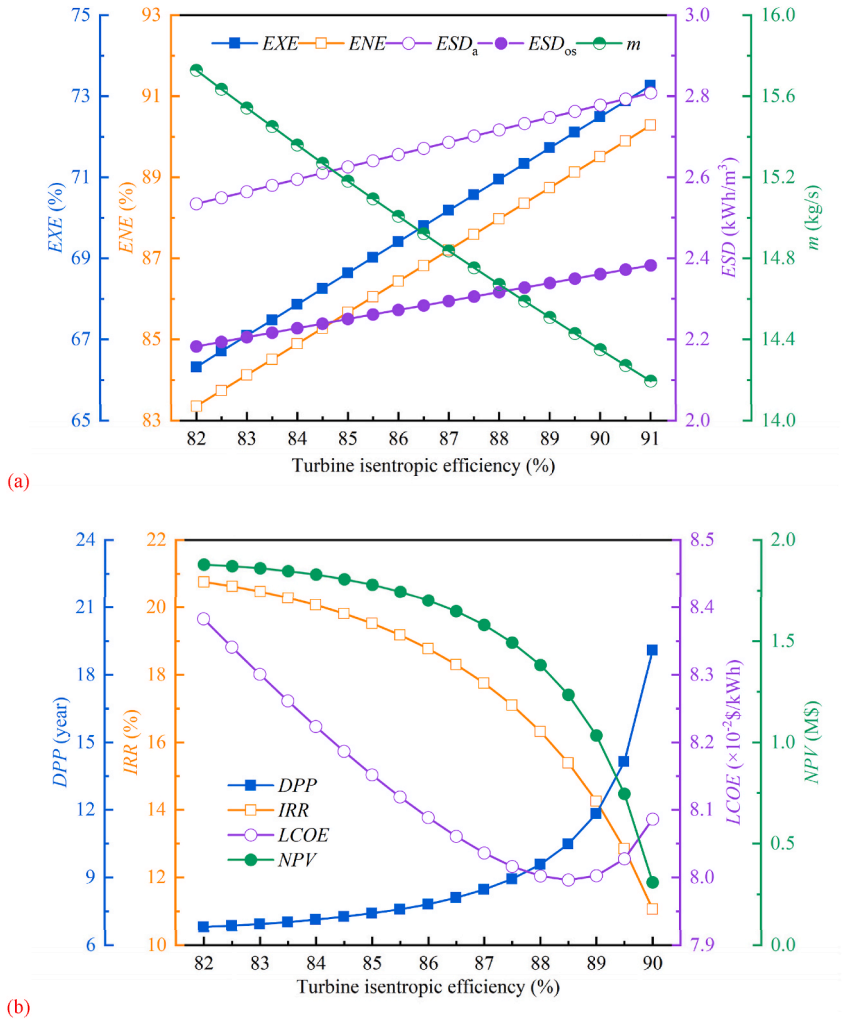

Fig. 9. Effect of turbine isentropic efficiency on system performance: (a) *ENE*, *EXE*, *ESD*, and *m*; (b) *IRR*, *DPP*, *LCOE*, and *NPV*.

5 MPa. Overall, increasing the air storage pressure is beneficial to the energy storage density but detrimental to the economic performance. A reasonable tradeoff of its value should be considered.

4.6.3. *Effect of heat exchanger efficiency*

In Fig. 7, there is a depiction of the effect of heat exchanger efficiency on the system performance. It is well-known that for a heat exchanger, the increased efficiency will make higher outlet temperature of cold side and lower outlet temperature of hot side. Thus, on the one hand, the air inlet temperature of compressors drops, resulting in the decrease of power consumption of compressors. On the other hand, the air inlet temperature of turbines rises due the increased temperature of hot water, which leads to the increase of power generation of turbines. Finally, based on these two aspects, the *ENE*, *EXE* and *ESD* increase and *m* decreases as the efficiency of heat exchanger increases. As can be seen from Fig. 7a, the *ENE* increases from 83.29 % to 87.11 % when the heat exchanger efficiency increases from 80 % to 90 %. As to the economic characteristic, when the heat exchanger efficiency increases, the costs of intercoolers and interheaters increase slightly since the heat exchanger area increases. However, the costs of compressors, turbines and ASR decrease due to the decreased mass flow rate of air. Taken together, it can be found from Fig. 7b that *LCOE* and *DPP* slightly decrease, and *NPV* slightly increases with heat exchanger efficiency. Additionally, it should be noted that the impact of heat exchanger efficiency on economic performance is minimal. When the heat exchanger efficiency increases from 80 % to 90 %, *LCOE* decreases from 0.0841 $/kWh to 0.0804 $/kWh.

4.6.4. *Effect of compressor isentropic efficiency*

Fig. 8 illustrates the correlation between compressor isentropic efficiency and system performance. As the compressor isentropic efficiency increases, the air outlet temperature of compressors deceases, which causes the drop in the temperature of compression heat. Hence, reduced turbine air inlet temperature results in an increase in air mass flow, which in turn leads to a decrement in the *ESD*.

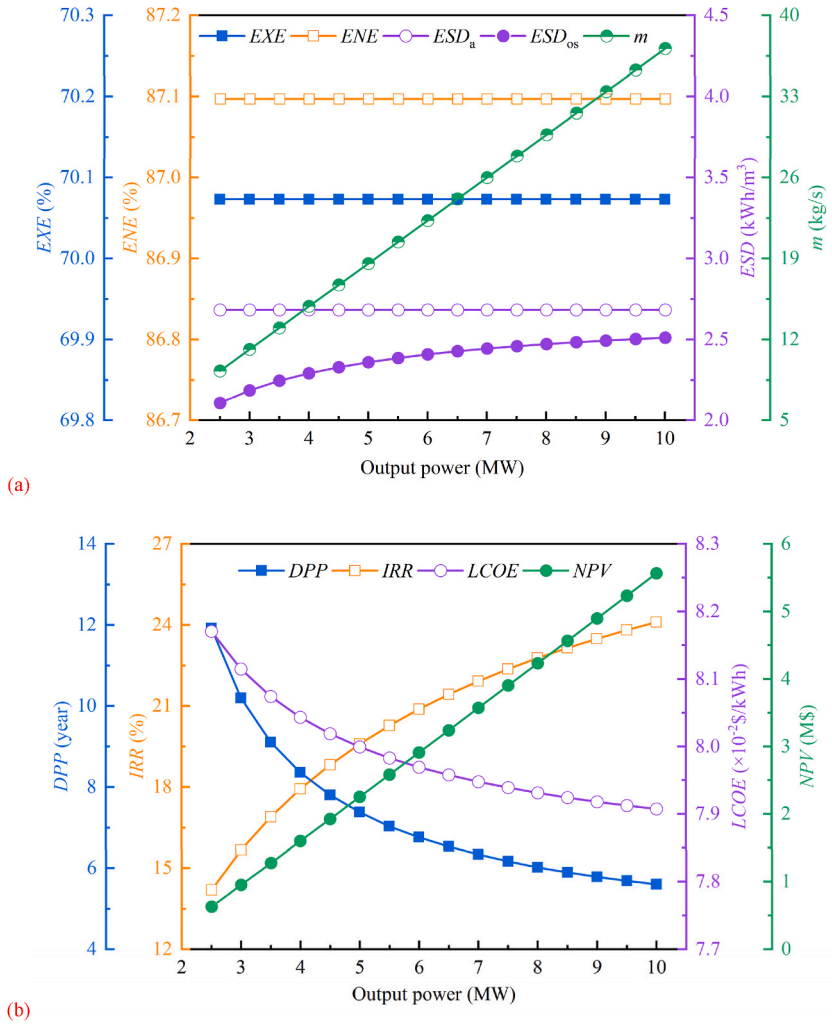

Fig. 10. Effect of output power on system performance: (a) *ENE*, *EXE*, *ESD*, and *m*; (b) *IRR*, *DPP*, *LCOE*, and *NPV*.

Furthermore, as the isentropic efficiency of the compressors rises, the total power consumption drops, which results in the increase in the *ENE* and *EXE*. From Fig. 8a, when the compressor isentropic efficiency increases from 82 % to 91 %, the *ENE* and *EXE* increase from 83.13 % to 66.23 %–88.81 % and 71.74 %, respectively. As for the economic performance, according to the cost equations given in Table 3, the cost of compressors, turbines and ASR increases due to the increased air mass flow rate caused by the increase of compressor isentropic efficiency. Therefore, *NPV* and *IRR* decrease, and *DPP* increases. It should be noted that an excessive value of compressor isentropic efficiency will make the *DPP* exceed the system lifespan and the *NPV* go negative. Additionally, the influence on *LCOE* is more complex. It is not only cost-related, but also depends on the system efficiency. With the ascendancy in the compressor's isentropic efficiency, its influence on increasing costs intensifies, while simultaneously its enhancement of system efficiency declines. Therefore, as depicted in Fig. 8b, there is an initial decrease followed by a subsequent rise in *LCOE* as the compressor isentropic efficiency rises.

4.6.5. *Effect of turbine isentropic efficiency*

Fig. 9 presents a graphic illustration of the influence of turbine isentropic efficiency on system performance. For the specified turbine power of 4 MW, the increase in turbine isentropic efficiency leads to less air mass flow rate and further, higher *ESD*. Simultaneously, the decreased air mass flow rate results in the decrease of power consumption of compressors, which causes the increase of *ENE* and *EXE*. From Fig. 9a, when the turbine isentropic efficiency increases from 82 % to 91 %, the *ENE* increases from 83.36 % to 90.29 %. It can be found from Fig. 9b that the influence of the turbine isentropic efficiency on the economic performance is similar to the influence of the compressor isentropic efficiency on that. Therefore, no further elaboration is presented here.

4.6.6. *Effect of output power capacity*

In Fig. 10, the influence of the output power capacity on the system's performance is demonstrated. From Fig. 10a that the air mass

flow rate increases with output power capacity linearly. However, the *ENE* and *EXE* is fixed because the thermodynamic parameters keep unchanged, and the specific power of turbines and compressors remains constant. Since the output power and the required volume of airbag increase synchronously, the ESD_a keeps unchanged with the variation of output power. Nevertheless, due to the unchanged required volume of heavy load, the ESD_{os} increases with the output power. It can be found Fig. 10b that increasing the output power is beneficial to the system's economic performance. This occurs due to, though the rise in output power leads to the increase in total investment cost, the total profit is growing faster than the total investment cost. When the output power increases from 2.5 MW to 10 MW, the *LCOE* decreases from 0.0817 $/kWh to 0.0791 $/kWh and DPP decreases from 11.92 years to 5.60 years. In summary, it can be drawn that increasing the output power capacity is favorable to both thermodynamic and economic performance. However, it is noteworthy that the output power capacity is restricted by the geographical conditions. A deeper or wider vertical mineshaft is needed if a higher output power is designed.

5. Conclusion

The paper introduces an innovative approach to isobaric adiabatic compressed air energy storage by combining the benefits of compressed air and gravity storage systems. The system can fully utilize the compressed air and reduce the waste of it. It also avoids the large exergy loss caused using throttle valves and improves the system's exergy and energy efficiency. The results of this study are given below.

(1) The energy analysis shows that the *ENE* and *EXE* are 87.10 % and 70.07 %, the ESD_a and ESD_{os} are 2.68 kWh/m^3 and 2.29 kWh/m^3, respectively.
(2) Exergy assessment demonstrates that among the primary components of the system, the turbine and compressor experience the largest exergy losses, accounting for 35.21 % and 30.98 % of the total exergy losses of the system, respectively. Among all the components of the system, the intercooler and interheater have lower exergy efficiency with the lowest 63.54 % and 50.60 %, respectively.
(3) The economic analysis shows that the *DPP*, *IRR*, *LCOE*, and *NPV* of the system are 8.36 years, 17.93 %, 0.0804$/kWh, and 1.60 M$, respectively.
(4) Parametric analysis shows that increasing the ambient temperature, heat exchanger efficiency, turbine isentropic efficiency and compressor isentropic efficiency will increase the *ENE* and *EXE* of the system. Raising the ambient temperature, heat exchanger efficiency and output power, reducing the air storage pressure all decrease the *LCOE* of the system.

CRediT authorship contribution statement

Ruifeng Cao: Writing – review & editing, Writing – original draft, Supervision, Project administration, Investigation, Funding acquisition, Conceptualization. **Zhe Wang:** Writing – review & editing, Writing – original draft, Validation, Software, Resources, Methodology, Investigation. **Hongliang Fan:** Writing – review & editing, Visualization, Software. **Ziqi Chen:** Writing – review & editing, Visualization, Software.

Declaration of competing interest

The authors declare that they have no known competing financial interests or personal relationships that could have appeared to influence the work reported in this paper.

Acknowledgments

This work was supported by Educational Committee of Jilin Province of China (No. JJKH20240137KJ).

Appendix

Table A1
Thermodynamic parameters at each state point of the proposed system

State	T (°C)	p (MPa)	m (kg/s)	h (kJ/kg)	s (kJ/kg · K)	$\dot{E}x$ (kW)
A1	25.00	0.10	14.86	298.45	6.86	0.00
A2	101.80	0.21	14.86	375.77	6.89	1040.86
A3	32.70	0.20	14.86	305.98	6.69	876.45
A4	111.46	0.41	14.86	385.31	6.72	1947.07
A5	33.67	0.40	14.86	306.54	6.50	1751.46
A6	112.76	0.81	14.86	386.13	6.52	2826.09
A7	33.80	0.79	14.86	305.83	6.30	2625.45

(*continued on next page*)

Table A1 (*continued*)

State	T (°C)	p (MPa)	m (kg/s)	h (kJ/kg)	s (kJ/kg · K)	$\dot{E}x$ (kW)
A8	113.09	1.62	14.86	385.50	6.32	3701.16
A9	33.83	1.57	14.86	304.21	6.09	3498.11
A10	113.42	3.22	14.86	383.99	6.12	4575.39
A11	33.86	3.12	14.86	301.03	5.89	4368.56
A12	33.86	3.12	14.86	301.03	5.89	4368.56
A13	93.07	3.03	14.86	363.06	6.08	4432.87
A14	25.05	1.32	14.86	295.73	6.12	3278.16
A15	92.19	1.28	14.86	364.53	6.33	3339.83
A16	24.89	0.56	14.86	297.29	6.37	2186.69
A17	92.17	0.54	14.86	365.55	6.58	2247.38
A18	25.14	0.24	14.86	298.28	6.62	1093.69
A19	92.20	0.23	14.86	366.02	6.83	1154.05
A20	25.27	0.10	14.86	298.73	6.87	0.00
W1	25.00	0.20	18.12	105.10	0.37	0.00
W2	25.00	0.20	3.70	105.10	0.37	0.00
W3	25.00	0.20	3.64	105.10	0.37	0.00
W4	25.00	0.20	3.61	105.10	0.37	0.00
W5	25.00	0.20	3.59	105.10	0.37	0.00
W6	25.00	0.20	3.58	105.10	0.37	0.00
W7	104.56	0.20	3.70	438.56	1.36	140.27
W8	104.26	0.20	3.64	437.27	1.35	137.00
W9	103.96	0.20	3.61	436.03	1.35	134.91
W10	102.80	0.20	3.59	431.10	1.34	130.66
W11	94.10	0.20	3.58	394.46	1.24	104.46
W12	101.96	0.20	18.12	427.59	1.33	646.02
W13	99.67	0.20	14.53	417.92	1.30	489.62
W14	99.67	0.20	3.58	417.92	1.30	120.74
W15	99.67	0.20	3.60	417.92	1.30	121.25
W16	99.67	0.20	3.63	417.92	1.30	122.47
W17	99.67	0.20	3.71	417.92	1.30	125.16
W18	32.61	0.20	3.58	136.91	0.47	1.43
W19	32.39	0.20	3.60	135.98	0.47	1.35
W20	32.53	0.20	3.63	136.58	0.47	1.42
W21	40.46	0.20	3.71	169.71	0.58	6.01
W22	34.54	0.20	14.53	144.98	0.50	9.08
W23	99.67	0.20	3.59	417.92	1.30	120.87
W24	99.67	0.20	18.12	417.92	1.30	610.49

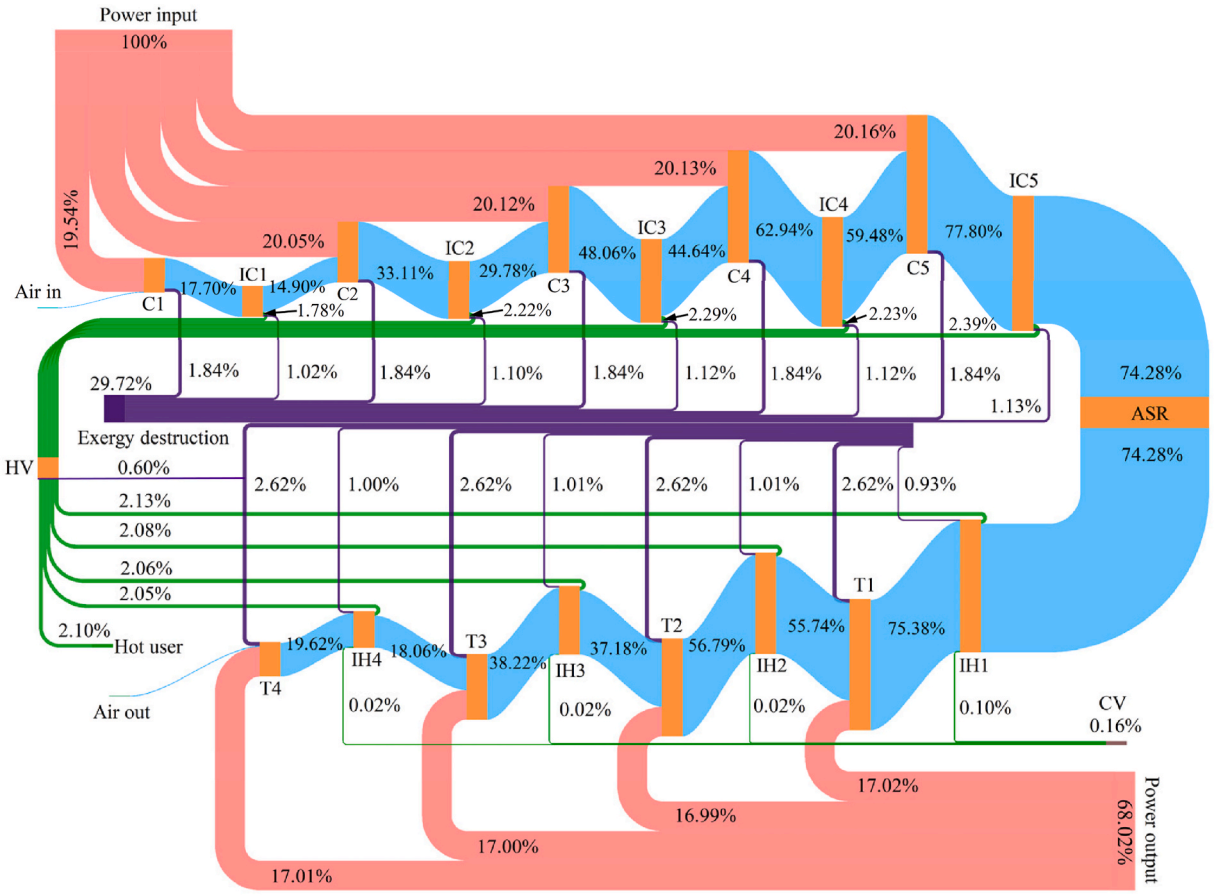

Fig. A1. Sankey diagram of the exergy transfer process of the system

Data availability

Data will be made available on request.

References

[1] X. Zhang, Z. Gao, B. Zhou, et al., Advanced compressed air energy storage systems: fundamentals and applications, Engineering 34 (2024) 246–269.
[2] P.C. Del Granado, Z. Pang, S.W. Wallace, Synergy of smart grids and hybrid distributed generation on the value of energy storage, Appl. Energy 170 (2016) 476–488.
[3] M. Khaljani, J. Harrison, D. Surplus, et al., A combined experimental and modelling investigation of an overground compressed-air energy storage system with a reversible liquid-piston gas compressor/expander, Energy Convers. Manag. 245 (2021) 114536.
[4] S. Rehman, L.M. Al-Hadhrami, M.M. Alam, Pumped hydro energy storage system: a technological review, Renew. Sustain. Energy Rev. 44 (2015) 586–598.
[5] J.P. Hoffstaedt, D.P.K. Truijen, J. Fahlbeck, et al., Low-head pumped hydro storage: a review of applicable technologies for design, grid integration, control and modelling, Renew. Sustain. Energy Rev. 158 (2022) 112119.
[6] E. Bazdar, M. Sameti, F. Nasiri, et al., Compressed air energy storage in integrated energy systems: a review, Renew. Sustain. Energy Rev. 167 (2022) 112701.
[7] A. Razmi, M. Soltani, M. Torabi, Investigation of an efficient and environmentally-friendly CCHP system based on CAES, ORC and compression-absorption refrigeration cycle: energy and exergy analysis, Energy Convers. Manag. 195 (2019) 1199–1211.
[8] W. Tong, Z. Lu, W. Chen, et al., Solid gravity energy storage: a review, J. Energy Storage 53 (2022) 105226.
[9] Z. Yang, J. Zhang, M.C.W. Kintner-Meyer, et al., Electrochemical energy storage for green grid, Chem. Rev. 111 (5) (2011) 3577–3613.
[10] K. Chen, D. Xue, Materials chemistry toward electrochemical energy storage, J. Mater. Chem. A 4 (20) (2016) 7522–7537.
[11] H.D. Yoo, E. Markevich, G. Salitra, et al., On the challenge of developing advanced technologies for electrochemical energy storage and conversion, Mater. Today 17 (3) (2014) 110–121.
[12] L. Chen, M. Xie, P. Zhao, et al., A novel isobaric adiabatic compressed air energy storage (IA-CAES) system on the base of volatile fluid, Appl. Energy 210 (2018) 198–210.
[13] A. Odukomaiya, E. Kokou, Z. Hussein, et al., Near-isothermal-isobaric compressed gas energy storage, J. Energy Storage 12 (2017) 276–287.
[14] Y. Zhang, J. Liu, S. Yin, et al., Design and performance analysis of a novel compressed air–liquid CO2 energy storage, Energy Convers. Manag. 301 (2024) 118068.
[15] W. Zhang, J. Ding, S. Yin, et al., Thermo-economic optimization of an artificial cavern compressed air energy storage with CO2 pressure stabilizing unit, Energy (2024) 130821.

[16] P. Zhao, W. Xu, W. He, et al., Thermo-economic analysis of a hybrid system based on combined heat-isobaric compressed air energy storage and humidification dehumidification desalination unit, Appl. Therm. Eng. 219 (2023) 119536.
[17] M.H. Nabat, M. Habibzadeh, A.S. Alsagri, et al., An investigation and multi-criteria optimization of an innovative compressed air energy storage, J. Energy Storage 76 (2024) 109645.
[18] Ł. Bartela, A. Skorek-Osikowska, S. Dykas, et al., Thermodynamic and economic assessment of compressed carbon dioxide energy storage systems using a post-mining underground infrastructure, Energy Convers. Manag. 241 (2021) 114297.
[19] X. Zhang, X. Xue, T. Zhang, et al., Thermodynamic and economic analysis of a novel gravity-enhanced compressed air energy storage system, Energy Sci. Eng. 10 (10) (2022) 4044–4060.
[20] B. Stanek, J. Ochmann, Ł. Bartela, et al., Isobaric tanks system for carbon dioxide energy storage–the performance analysis, J. Energy Storage 52 (2022) 104826.
[21] H. Du, X. Bian, W. Xiong, Design and energy characteristic analysis of a flexible isobaric strain-energy compressed-air storage device, J. Energy Storage 50 (2022) 104312.
[22] K.J. Rolland, T. Nitsche, M. Budt, et al., Isobaric storage of compressed air: introduction of a novel concept based on phase change materials and pressure equalizing modules, J. Energy Storage 61 (2023) 106778.
[23] Y. Mazloum, H. Sayah, M. Nemer, Exergy analysis and exergoeconomic optimization of a constant-pressure adiabatic compressed air energy storage system, J. Energy Storage 14 (2017) 192–202.
[24] H. Wang, Z. Tong, X. Dong, et al., Design and energy saving analysis of a novel isobaric compressed air storage device in pneumatic systems, J. Energy Storage 38 (2021) 102614.
[25] S.M. Alirahmi, A.R. Razmi, A. Arabkoohsar, Comprehensive assessment and multi-objective optimization of a green concept based on a combination of hydrogen and compressed air energy storage (CAES) systems, Renew. Sustain. Energy Rev. 142 (2021) 110850.
[26] D.N. Özen, E.H. Güleryüz, A.M. Acılar, Advanced exergo-economic analysis of an advanced adiabatic compressed air energy storage system with the modified productive structure analysis method and multi-objective optimization study, J. Energy Storage 81 (2024) 110380.
[27] E. Yao, L. Zhong, R. Li, et al., Enhanced compression heat recovery of coupling thermochemical conversion to trigenerative compressed air energy storage system: systematic sensitivity analysis and multi-objective optimization, J. Energy Storage 68 (2023) 107738.
[28] S.M. Alirahmi, S.B. Mousavi, A.R. Razmi, et al., A comprehensive techno-economic analysis and multi-criteria optimization of a compressed air energy storage (CAES) hybridized with solar and desalination units, Energy Convers. Manag. 236 (2021) 114053.
[29] L. Chen, D. Cheng, P. Tang, et al., Combination of compressed air energy storage and kalina 11 cycles for sustainable energy provision; energy, exergy, and economic analysis, Int. J. Energy Res. 45 (14) (2021) 19962–19984.
[30] S.B. Mousavi, M. Adib, M. Soltani, et al., Transient thermodynamic modeling and economic analysis of an adiabatic compressed air energy storage (A-CAES) based on Cascade packed bed thermal energy storage with encapsulated phase change materials, Energy Convers. Manag. 243 (2021) 114379.
[31] H. Chen, H. Wang, R. Li, et al., Thermo-dynamic and economic analysis of a novel pumped hydro-compressed air energy storage system combined with compressed air energy storage system as a spray system, Energy 280 (2023) 128134.
[32] A. Razmi, M. Soltani, C. Aghanajafi, et al., Thermodynamic and economic investigation of a novel integration of the absorption-recompression refrigeration system with compressed air energy storage (CAES), Energy Convers. Manag. 187 (2019) 262–273.
[33] X. Xue, J. Li, J. Liu, et al., Performance evaluation of a conceptual compressed air energy storage system coupled with a biomass integrated gasification combined cycle, Energy 247 (2022) 123442.
[34] R. Cao, Y. Wang, W. Li, et al., Thermodynamics analysis of a hybrid system based on a combination of hydrogen fueled compressed air energy storage system and water electrolysis hydrogen generator, Int. J. Hydrogen Energy 48 (63) (2023) 24492–24503.
[35] M.H. Nabat, M. Zeynalian, A.R. Razmi, et al., Energy, exergy, and economic analyses of an innovative energy storage system; liquid air energy storage (LAES) combined with high-temperature thermal energy storage (HTES), Energy Convers. Manag. 226 (2020) 113486.
[36] E. Assareh, M. Jafari, S. Keykhah, et al., Transient thermodynamic modeling and economic assessment of cogeneration system based on compressed air energy storage and multi-effect desalination, J. Energy Storage 55 (2022) 105683.
[37] X. Xu, Z. Ye, Q. Qian, Economic, exergoeconomic analyses of a novel compressed air energy storage-based cogeneration, J. Energy Storage 51 (2022) 104333.
[38] R. Du, Y. He, H. Chen, et al., Performance and economy of trigenerative adiabatic compressed air energy storage system based on multi-parameter analysis, Energy 238 (2022) 121695.
[39] R. Cao, S. Wang, W. Li, et al., Thermodynamic and techno-economic evaluation of a CAES based cogeneration system integrated with high-temperature thermal energy storage and ammonia absorption refrigeration, Case Stud. Therm. Eng. 56 (2024) 104293.
[40] R. Cao, W. Li, X. Cong, et al., Energy, exergy and economic (3E) analysis and multi-objective optimization of a combined cycle power system integrating compressed air energy storage and high-temperature thermal energy storage, Appl. Therm. Eng. 238 (2024) 122077.
[41] W. Liang, Z. Yu, W. Liu, et al., Investigation of a novel near-zero emission poly-generation system based on biomass gasification and SOFC: a thermodynamic and exergoeconomic evaluation, Energy 282 (2023) 128822.
[42] P. Li, Q. Hu, G. Li, et al., Research on thermo-economic characteristics of a combined cooling, heating and power system based on advanced adiabatic compressed air energy storage, J. Energy Storage 47 (2022) 103590.
[43] S. Wu, C. Zhou, E. Doroodchi, et al., Techno-economic analysis of an integrated liquid air and thermochemical energy storage system, Energy Convers. Manag. 205 (2020) 112341.
[44] Z. Han, Y. Sun, P. Li, Thermo-economic analysis and optimization of a combined cooling, heating and power system based on advanced adiabatic compressed air energy storage, Energy Convers. Manag. 212 (2020) 112811.
[45] L. Zhong, E. Yao, Y. Hu, et al., Thermo-economic analysis of a novel system integrating compressed air and thermochemical energy storage with solid oxide fuel cell-gas turbine, Energy Convers. Manag. 252 (2022) 115114.
[46] B. Yan, S. Xue, Y. Li, et al., Gas-fired combined cooling, heating and power (CCHP) in beijing: a techno-economic analysis, Renew. Sustain. Energy Rev. 63 (2016) 118–131.
[47] A. Arabkoohsar, G.B. Andresen, Design and optimization of a novel system for trigeneration, Energy 168 (2019) 247–260.
[48] V. Zare, S.M.S. Mahmoudi, M. Yari, An exergoeconomic investigation of waste heat recovery from the gas turbine-modular helium reactor (GT-MHR) employing an ammonia-water power/cooling cycle, Energy 61 (2013) 397–409.
[49] R. Cao, W. Li, Z. Chen, et al., Development and assessment of a novel isobaric compressed hydrogen energy storage system integrated with pumped hydro storage and high-pressure proton exchange membrane water electrolyzer, Energy 294 (2024) 130798.
[50] F. Salomone, E. Giglio, D. Ferrero, et al., Techno-economic modelling of a power-to-gas system based on SOEC electrolysis and CO2 methanation in a RES-Based electric grid, Chem. Eng. J. 377 (2019) 120233.
[51] E. Yao, H. Wang, L. Wang, et al., Multi-objective optimization and exergoeconomic analysis of a combined cooling, heating and power based compressed air energy storage system, Energy Convers. Manag. 138 (2017) 199–209.
[52] Z. Wu, P. Zhu, J. Yao, et al., Combined biomass gasification, SOFC, IC engine, and waste heat recovery system for power and heat generation: energy, exergy, exergoeconomic, environmental (4E) evaluations, Appl. Energy 279 (2020) 115794.
[53] A.R. Razmi, M. Janbaz, Exergoeconomic assessment with reliability consideration of a green cogeneration system based on compressed air energy storage (CAES), Energy Convers. Manag. 204 (2020) 112320.